

Intravascular fibrin molecular imaging improves the detection of unhealed stents assessed by optical coherence tomography *in vivo*

Tetsuya Hara^{1†‡}, Giovanni J. Ughi^{2‡}, Jason R. McCarthy³, S. Sibel Erdem^{3†}, Adam Mauskopf¹, Samantha C. Lyon², Ali M. Fard², Elazer R. Edelman⁴, Guillermo J. Tearney^{2§*}, and Farouc A. Jaffer^{1,2§*}

¹Cardiovascular Research Center, Massachusetts General Hospital, Harvard Medical School, Boston, MA, USA; ²Wellman Center for Photomedicine, Massachusetts General Hospital, Harvard Medical School, Boston, MA, USA; ³Center for System Biology, Massachusetts General Hospital, Harvard Medical School, Boston, MA, USA; and ⁴Massachusetts Institute of Technology, Cambridge, MA, USA

Received 15 June 2015; revised 14 September 2015; accepted 21 November 2015; online publish-ahead-of-print 18 December 2015

See page 456 for the editorial comment on this article (doi:1093/eurheartj/ehv768)

Aims

Fibrin deposition and absent endothelium characterize unhealed stents that are at heightened risk of stent thrombosis. Optical coherence tomography (OCT) is increasingly used for assessing stent tissue coverage as a measure of healed stents, but cannot precisely identify whether overlying tissue represents physiological neointima. Here we assessed and compared fibrin deposition and persistence on bare metal stent (BMS) and drug-eluting stent (DES) using near-infrared fluorescence (NIRF) molecular imaging *in vivo*, in combination with simultaneous OCT stent coverage.

Methods and results

Rabbits underwent implantation of one BMS and one DES without overlap in the infrarenal aorta ($N = 20$ 3.5×12 mm). At Days 7 and/or 28, intravascular NIRF-OCT was performed following the injection of fibrin-targeted NIRF molecular imaging agent FTP11-CyAm7. Intravascular NIRF-OCT enabled high-resolution imaging of fibrin overlying stent struts *in vivo*, as validated by histopathology. Compared with BMS, DES showed greater fibrin deposition and fibrin persistence at Days 7 and 28 ($P < 0.01$ vs. BMS). Notably, for edge stent struts identified as covered by OCT on Day 7, $92.8 \pm 9.5\%$ of DES and $55.8 \pm 23.6\%$ of BMS struts were NIRF fibrin positive ($P < 0.001$). At Day 28, $18.6 \pm 10.6\%$ (DES) and $5.1 \pm 8.7\%$ (BMS) of OCT-covered struts remained fibrin positive ($P < 0.001$).

Conclusion

Intravascular NIRF fibrin molecular imaging improves the detection of unhealed stents, using clinically translatable technology that complements OCT. A sizeable percentage of struts deemed covered by OCT are actually covered by fibrin, particularly in DES, and therefore such stents might remain prothrombotic. These findings have implications for the specificity of standalone clinical OCT assessments of stent healing.

Keywords

Stent thrombosis • Fibrin • Molecular imaging • Optical coherence tomography

* Corresponding author. Tel: +1 617 724 9353, Fax: +1 617 860 3180, Email: fjaffer@mgh.harvard.edu (F.A.J.); gtearney@mgh.harvard.edu (G.J.T)

† Present address: Division of Cardiology, Kobe University Graduate School of Medicine, Kobe, Japan; Dr. Erdem: İstanbul Medipol University, International School of Medicine and Regenerative and Restorative Medicine Research Center (REMER), İstanbul, Turkey.

‡ These authors contributed equally to this work.

§ These authors share senior authorship.

Published on behalf of the European Society of Cardiology. All rights reserved. © The Author 2015. For permissions please email: journals.permissions@oup.com.

Translational perspective

Optical coherence tomography (OCT) is increasingly used to understand coronary stent coverage and healing, and inform mechanisms and risks regarding stent thrombosis. Here we demonstrate, via *in vivo* NIRF fibrin molecular imaging agent and catheter technology, that stent coverage by OCT may actually reflect coverage by fibrin, a pro-thrombotic material, particularly at the edges of drug-eluting stents. Translationally, an MRI version of the NIRF fibrin-imaging agent has already been tested in Phase II trials, and near-infrared fluorophores such as indocyanine green are clinically approved. From a catheter standpoint, clinical intracoronary testing of a NIRF-OCT catheter is underway. Therefore, NIRF-OCT fibrin imaging has translational potential and could help assess the healing of implanted coronary stents in preclinical and clinical use.

Introduction

Stent thrombosis is a life-threatening complication of coronary artery stents that occurs when a blood clot forms acutely within a stent. Patients remain at risk of stent thrombosis from both bare metal stents (BMS) and drug-eluting stents (DES), despite dual antiplatelet therapy (DAPT).¹ Seminal pathology studies have revealed that stents with delayed healing, characterized by incomplete endothelialization and pro-thrombotic fibrin deposition, are at heightened risk of stent thrombosis.^{2,3} Furthermore, a recent landmark clinical study shows that the risk of stent thrombosis persists for years, and is reduced, but not eliminated, by prolonged DAPT.⁴ Therefore, the questions of which subjects remain at risk for stent thrombosis, and which subjects can safely stop DAPT, remain of paramount importance.

Assessment of stent endothelialization and fibrin deposition has historically been performed at autopsy.^{2,3} Recently however, investigators have applied high-resolution optical coherence tomography (OCT) to assess tissue overlying stent struts, termed 'OCT strut coverage', as a surrogate for coronary stent healing, and to potentially inform the risk of stent thrombosis. However, limitations of OCT including insufficient resolution and a lack of fibrin-specific tissue contrast^{5,6} might limit the ability of OCT to accurately identify healed stents and to predict clinical stent thrombosis. These limitations might underlie the unclear association between measures of OCT strut coverage and subsequent clinical events. Therefore, a strategy to rapidly, comprehensively, and quantitatively assess fibrin deposition on coronary stents *in vivo*, in combination with simultaneous tissue coverage assessment by OCT, could significantly advance our knowledge regarding stent healing, and potentially improve the prediction of stent thrombosis.

Molecular imaging offers the potential to detect fibrin at high resolution using intravascular near-infrared fluorescence (NIRF)-OCT imaging *in vivo*. This concept was recently introduced in a single timepoint study that imaged stents that were soaked *ex vivo* with high concentrations of NIR fluorescent plasma, and then implanted in rabbit arteries and immediately imaged.⁷ This preliminary concept however was not informative for clinically translatable imaging, as it (i) did not demonstrate that an intravenously injectable fibrin-targeted agent could stably bind implanted stents under conditions of arterial blood flow; (ii) did not assess whether physiological levels of fibrin following stent implantation could be detected *in vivo*, especially in subacutely placed stents with lower fibrin levels; and (iii) utilized a nanomaterial imaging agent with limited translatability.⁸

In this translational study, we harnessed intravascular NIRF-OCT fibrin molecular-structural imaging to identify the healing status of implanted DES and BMS, compared with standalone OCT-tissue

coverage assessment, and further utilized serial NIRF-OCT to assess fibrin persistence over time in single stents *in vivo*.

Methods

The Institutional Animal Use and Care Committee at Massachusetts General Hospital approved all animal studies (#2004P001401). Discarded human blood products were obtained using a Partners institutional review board-approved protocol (#2013N000015). Full details are described in Supplementary material online.

Coronary stent implantation in rabbits

Coronary BMS (ML VISION, 3.5 × 12 mm, Abbott Vascular) or everolimus-eluting DES (XIENCE V, 3.5 × 12 mm, Abbott Vascular) was implanted into the infra-renal aorta in New Zealand white rabbits, which is the same calibre as a human coronary artery. The orientation of BMS and DES (proximal or distal segments of the abdominal aorta) was chosen randomly.

Intravascular near-infrared fluorescence-optical coherence tomography molecular-structural imaging *in vivo*

The intravascular NIRF-OCT imaging system and catheter have been previously described.⁷ See Supplementary material online, Figures S1–S2 for details on the imaging system, catheter, NIRF, and OCT image analysis, and distance-correction of the fluorescence signal to permit quantitative NIRF comparison of stents at different time points and among animals.⁹

Statistical analysis

Results are expressed as mean ± SD. A value of $P < 0.05$ was considered statistically significant for two and multiple groups comparison. Two-sided P -values are reported. For multiple testing, adjusted P -values are reported.

Results

Synthesis, binding, and blood half-life of the fibrin-targeted near-infrared fluorescence agent FTP11-CyAm7

We recently developed a fibrin-targeted NIRF imaging agent (FTP11-Cy7) and validated it in murine thrombosis.¹⁰ For the scale-up synthesis to image fibrin in rabbit, we conjugated an in-house NIR fluorophore (CyAm7, ex/em 744/769 nm) to a validated fibrin-binding peptide^{10,11} (Supplementary material online, Figure S3A). *In vitro*, FTP11-CyAm7 enhanced fibrin-rich clots from both rabbit and human plasma, significantly above free CyAm7 control [target-to-background ratio (TBR) = 20.5 ± 3.5 vs. 3.4 ± 1.4 for rabbit clots, 25.1 ± 5.2 vs. 2.1 ± 0.2 for human clots, $P < 0.0001$,

respectively, Supplementary material online, Figure S3B]. The blood half-life of FTP11-CyAm7 was 8.1 min in rabbits (95% CI, 6.5–10.9, Supplementary material online, Figure S3C).

In vivo near-infrared fluorescence-optical coherence tomography of fibrin deposition on coronary stent struts

A total of 20 stents ($n = 13$ BMS, $n = 7$ DES) were implanted and 28 NIRF-OCT imaging pullbacks of coronary stents (17 BMS, 11 DES) including serial imaging were analysed (Supplementary material online, Figure S1). Intravascular NIRF-OCT imaging was performed prior to and then 2 h after intravenous injection of FTP11-CyAm7. Minimal background NIRF signal was observed prior to FTP11-CyAm7 injection (data not shown), consistent with low autofluorescence in the NIR window.¹² In contrast, the post-injection images revealed elevated NIRF signal surrounding stent struts (Figure 1). Higher NIRF fibrin signal was evident at stent edges. Axial NIRF-OCT fusion images demonstrated fibrin deposition on and around stent struts (Figure 1A and B).

Fluorescence microscopy of longitudinally opened stents confirmed similar localization of NIRF-fibrin signal within the stent (Figure 1A). Histological evaluation demonstrated that the FTP11-CyAm7 signal colocalized with fibrin deposition identified by

Carstairs' stain and fibrin immunostaining (Figure 1C and D). Near-infrared fluorescence fibrin signal localized specifically near stent struts, extending prior findings of fibrin deposition patterns in a flow loop model¹³ and histopathological studies.^{2,3,14,15} These results indicate that NIRF-OCT fibrin molecular imaging can accurately assess fibrin deposition in stents *in vivo*.

Optical coherence tomography assessment of tissue coverage on coronary stent struts *in vivo*

The OCT per strut analyses of coverage and malapposition are summarized and shown in Table 1. Optical coherence tomography revealed that DES exhibited greater rates of uncovered stent struts compared with BMS at both Day 7 ($P < 0.001$) and Day 28 ($P < 0.05$), consistent with prior studies.^{2,3,14–16}

Bare metal stent fibrin dissipates from Days 7 to 28, as assessed by near-infrared fluorescence-optical coherence tomography molecular-structural imaging

To assess the temporal dynamics of fibrin deposition on BMS *in vivo*, we next imaged BMS of two different healing stages (Days 7 and 28)

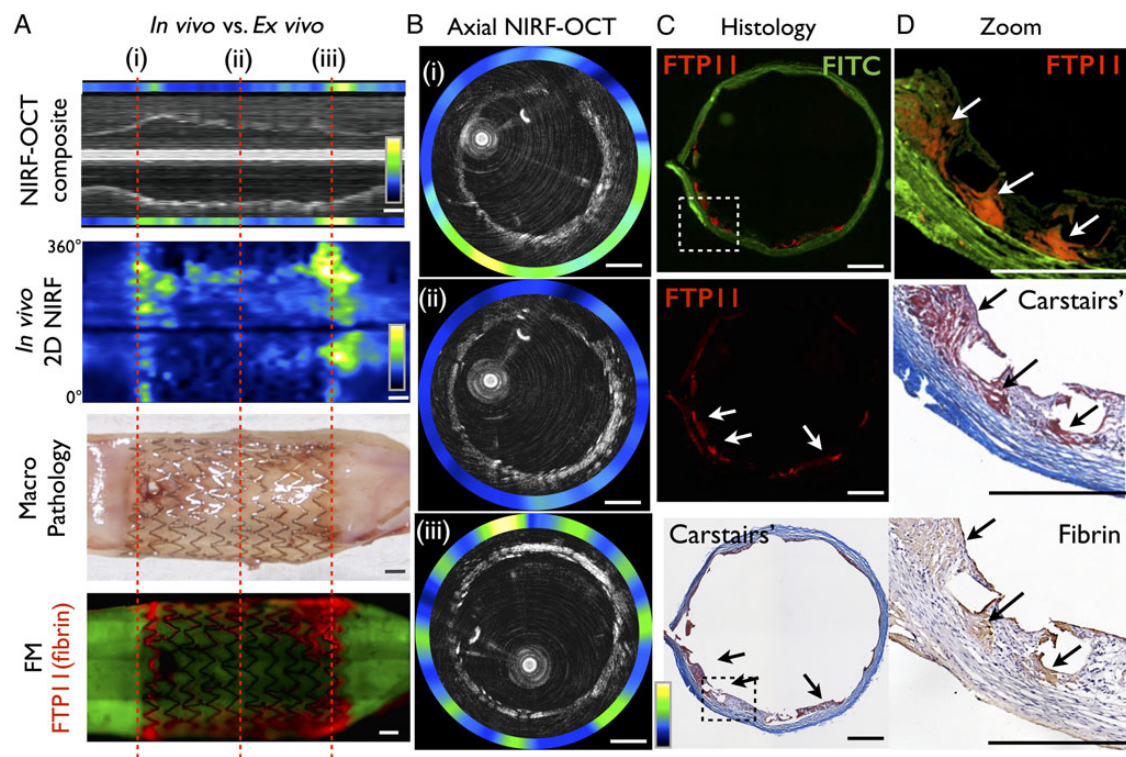


Figure 1 Intravascular near-infrared fluorescence-optical coherence tomography imaging of fibrin deposition on stents. Rabbits underwent implantation of a 3.5 mm diameter bare metal stent in the aorta. At Day 7, the fibrin molecular imaging agent FTP11-CyAm7 was i.v. injected, followed by near-infrared fluorescence-optical coherence tomography. (A) *In vivo* 2D near-infrared fluorescence map of stent (upper two rows) and corresponding *ex vivo* imaging after longitudinally opened (lower two rows). (B) Representative cross-sectional near-infrared fluorescence-optical coherence tomography images at the stent distal edge (i), middle (ii), and proximal edge (iii). (C and D) Histological sections of the proximal stent edge (dotted line in A (i)) are shown. Near-infrared fluorescence signal of FTP11-CyAm7 (red) co-localized with fibrin (bright red in Carstairs' staining) and fibrin immunostaining. All scale bars = 1 mm.

implanted in the infrarenal aorta of rabbits ($N = 3$). We selected the Days 7 and 28 time points in rabbits to correspond to human time-points for stent healing at 1 month (subacute) and 6 months (late),

respectively.^{16,17} *In vivo* NIRF-OCT molecular imaging of fibrin in Day 7 BMS showed elevated NIRF signal, primarily at the stent edges. In contrast, little NIRF fibrin signal was observed in Day 28 BMS ($P < 0.0001$, Supplementary material online, Figure S4).

Table 1 Optical coherence tomography stent whole struts analyses

	BMS	DES	P-value
Day 7	N = 10	N = 7	
Total struts analysed	3675	2369	
% covered struts	33.3 ± 1.79	8.39 ± 1.32	*0.0006
% malapposed struts	1.34 ± 0.578	4.07 ± 1.77	0.06
Day 28	N = 4	N = 4	
Total struts analysed	2539	1375	
% covered struts	92.8 ± 2.98	85.8 ± 2.79	*0.04
% malapposed struts	0.138 ± 0.102	0.350 ± 0.260	0.42

BMS, bare metal stent; DES, drug-eluting stent.

* $P < 0.05$ indicates significant differences between stent groups.

Greater fibrin deposition is evident in drug-eluting stent compared with bare metal stent at Day 7 *in vivo*

It remains unclear whether there are differences in the subacute stent thrombosis rates between BMS and DES. We compared the fibrin deposition between BMS and DES 7 days after implantation ($n = 7$ BMS, $n = 7$ DES), where Day 7 in the rabbit corresponds to 1 month in humans.¹⁶ We observed significantly greater NIRF fibrin signal in DES than BMS at Day 7 after stent implantation ($P < 0.0001$, Figure 2). Drug-eluting stent at Day 7 also demonstrated an edge-enhanced NIRF distribution pattern similar to BMS, but greater in magnitude. In addition, we also observed relatively higher NIRF fibrin signal throughout the mid stent segment in DES compared with BMS (Figure 2).

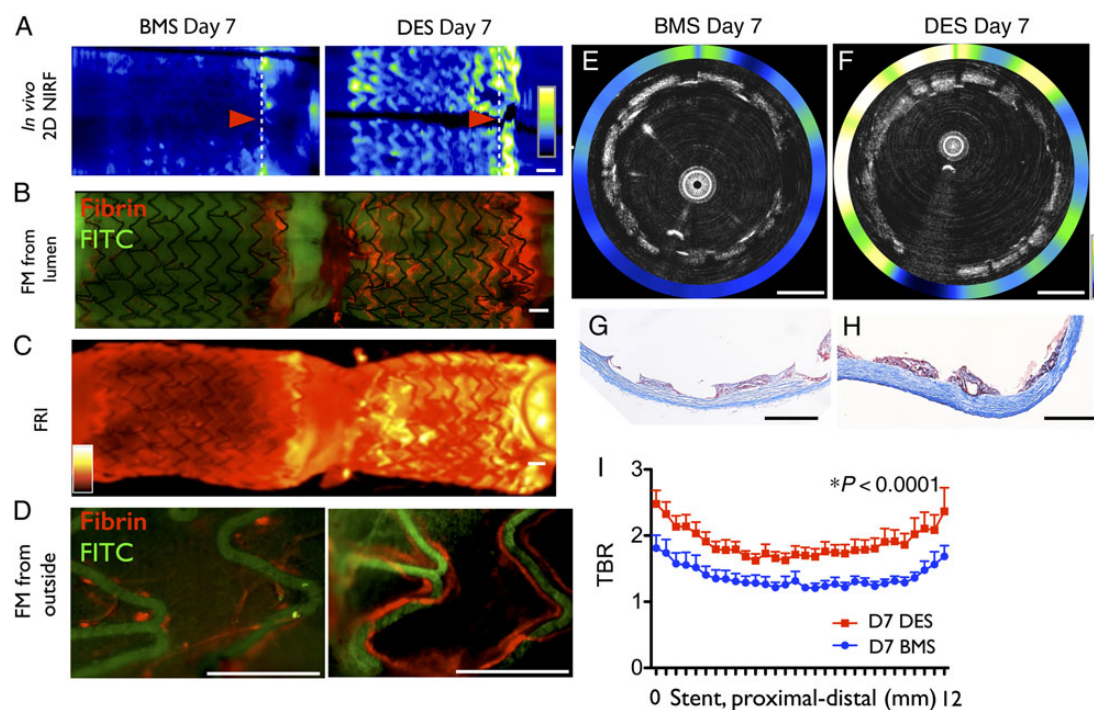


Figure 2 Drug-eluting stent exhibit greater fibrin deposition than bare metal stent at Day 7 *in vivo*. Rabbits were implanted with a nonoverlapping bare metal stent and drug-eluting stent, and then imaged with near-infrared fluorescence-optical coherence tomography after FTP11-CyAm7 fibrin agent injection on Day 7. (A) *In vivo* 2D near-infrared fluorescence map with bare metal stent (left) and drug-eluting stent (right), corresponding (B) fluorescence microscopy after longitudinally opening stents, (C) fluorescence reflectance imaging and (D) fluorescence microscopy from the outside. Representative *in vivo* axial near-infrared fluorescence-optical coherence tomography images of (E) Day 7 bare metal stent and (F) Day 7 drug-eluting stent at the distal edge (arrowhead in A). Carstairs' stain (G and H) demonstrates that some areas of bare metal stent tissue coverage are fibrin-negative, but almost all areas of drug-eluting stent tissue coverage are fibrin-positive. (I) *In vivo* near-infrared fluorescence-fibrin signal from the proximal to distal stent edge of bare metal stent and drug-eluting stent ($n = 7$ BMS, $n = 7$ drug-eluting stent). FRI, fluorescence reflectance imaging; FITC, fluorescein isothiocyanate autofluorescence. Scale bars = 1 mm.

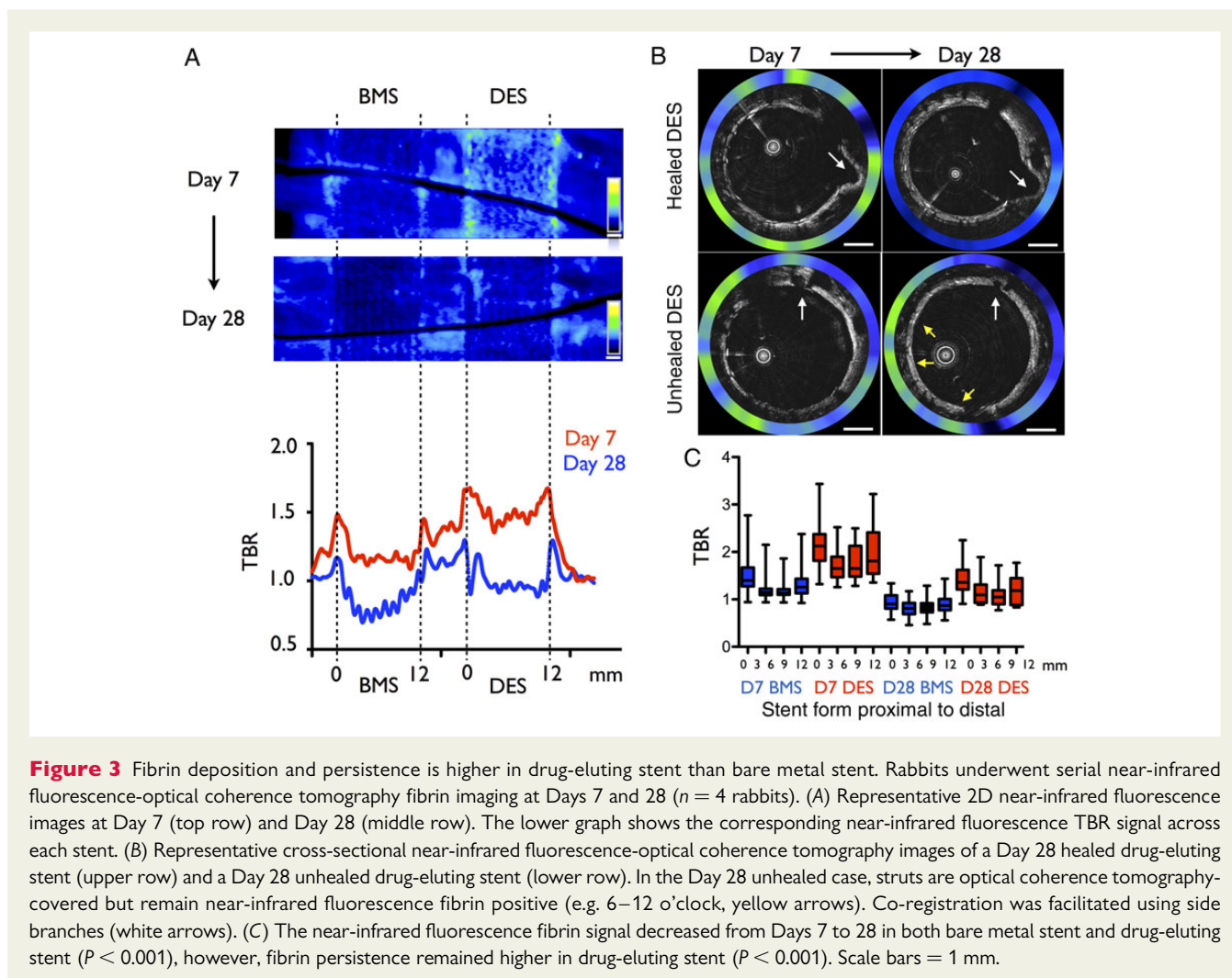
Comparison of fibrin dissipation rates in bare metal stent and drug-eluting stent *in vivo*

The rate of fibrin dissipation in coronary stents *in vivo* is unknown. To assess temporal changes in fibrin deposition in individual BMS and DES *in vivo*, a subset of rabbits ($N = 4$) underwent serial NIRF-OCT fibrin imaging at Day 7 and then again at Day 28 post-stent implantation. We first confirmed that at Day 28, minimal residual NIRF signal was remnant from the initial Day 7 FTP11-CyAm7 injection (Supplementary material online, Figure S5). Co-registration of serially obtained Days 7 and 28 NIRF-OCT datasets revealed that both BMS and DES showed reductions in fibrin-NIRF signal (Figure 3A and B). Day 28 DES exhibited quantitatively greater fibrin deposition at all zones of the stent (edges, mid-section) compared with matched Day 28 BMS ($P < 0.0001$, Figure 3C). En face whole mount fluorescence microscopy corroborated higher fibrin-NIRF signal in Day 28 DES (Supplementary material online, Figure S6). Furthermore, en face microscopy of DAPI-stained tissue revealed less cellularity in Day 28 DES vs. Day 28 BMS. Carstairs' fibrin staining also confirmed sustained peri-strut

fibrin deposition (Supplementary material online, Figure S6C and D), as previously reported.¹⁴

A portion of optical coherence tomography-covered edge stent struts is near-infrared fluorescence-fibrin positive, particularly in drug-eluting stent

While OCT-determined stent strut coverage is presumed to indicate a healed stent strut, *ex vivo* studies reveal that OCT tissue coverage can in fact represent coverage by fibrin or inflammatory cells, rather than physiological tissue, leading to an uncertainty regarding the healing state of stents.⁶ Although strut coverage was highest at the stent edges as previously reported,¹⁴ the NIRF fibrin signal was also highest at the stent edges (outer 2 mm). Therefore, we analysed the extent of fibrin-rich neointima at Days 7 and 28 at the stent edges ($n = 8$ for Day 7 stents, $n = 8$ for Day 28 stents). Interestingly, most OCT-covered tissue on Day 7 DES struts was fibrin-rich ($92.8 \pm 9.5\%$ of edge struts), and significantly higher than Day 7 BMS (fibrin-positive struts $55.8 \pm 23.6\%$, $P = 0.0017$).



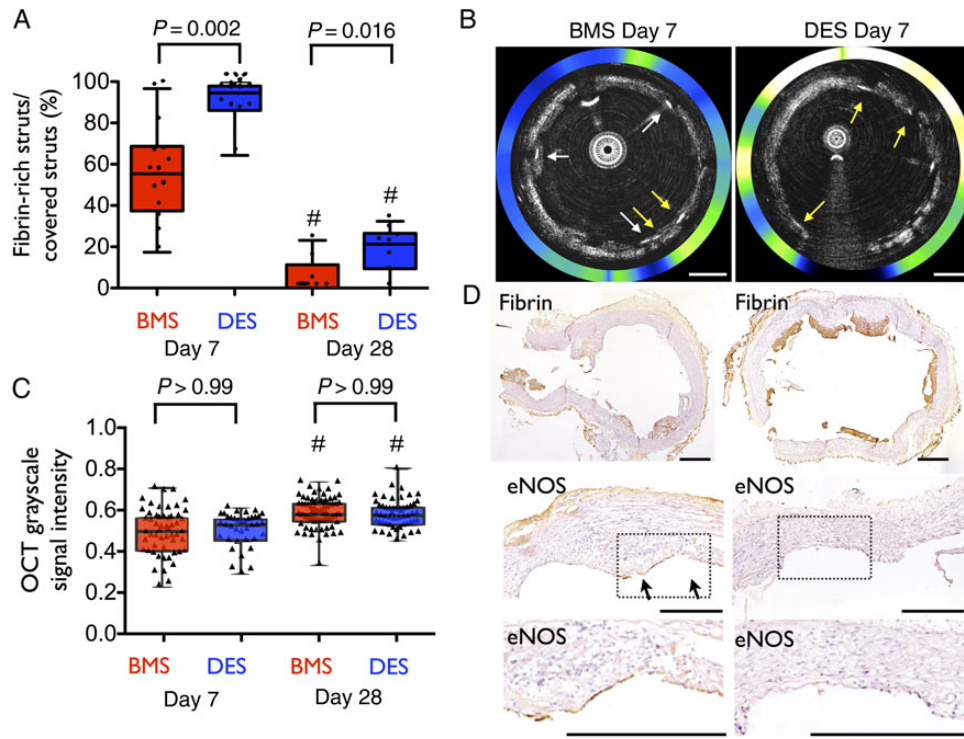


Figure 4 Near-infrared fluorescence molecular imaging identifies optical coherence tomography-covered, but unhealed fibrin-rich struts *in vivo*. (A) The percentage of fibrin-rich neointimal tissue at stent edges was assessed by near-infrared fluorescence-optical coherence tomography. Drug-eluting stent showed significantly higher rate of fibrin-rich covering tissue than bare metal stent. (B) Near-infrared fluorescence-optical coherence tomography images of bare metal stent and drug-eluting stent at Day 7 revealed a diversity of fibrin-rich (yellow arrows) and fibrin-negative (white arrows) struts, even within a single cross-section. (C) Grayscale optical coherence tomography intensity was similar between bare metal stent and drug-eluting stent at both Days 7 and 28 timepoints ($n = 4$ stents in each group), despite higher fibrin signal in DES > BMS at both Days 7 and 28 at the stent edges. (D) Fibrin immunostaining and endothelial nitric oxide synthase immunostaining (magnified images at bottom) are shown. Most Day 7 drug-eluting stent edge tissue coverage is fibrin-rich and lacks endothelial nitric oxide synthase expression, in contradistinction to Day 7 bare metal stent. $^{\#}P < 0.05$ vs. respective Day 7.

At Day 28, fibrin on DES edge struts was three-fold more prevalent than on BMS ($18.6 \pm 10.6\%$ of DES vs. $5.1 \pm 8.7\%$ of BMS, $P = 0.0156$, Figure 4A). These findings were supported by histological analyses (Figure 4D). The functional endothelial cell marker endothelial nitric oxide synthase was well expressed in areas of BMS neointima, in contrast to DES neointima, consistent with prior studies.¹⁵

Optical coherence tomography grayscale signal intensity and near-infrared fluorescence-fibrin relationships

While differences in OCT grayscale signal intensity (GSI) of stent strut tissue coverage might distinguish fibrin,¹⁸ we found that the OCT GSI was similar between Day 7 BMS and DES (BMS 0.50 ± 0.11 vs. DES 0.51 ± 0.08 , $P > 0.99$), and between Day 28 BMS and DES (0.59 ± 0.07 vs. 0.58 ± 0.07 , $P > 0.99$, Figure 4C), despite higher NIRF-fibrin in DES > BMS at each time point. Significantly higher GSI was observed in Day 28 mature neointima compared with Day 7 immature neointima ($P < 0.0001$ for

BMS and $P = 0.0011$ for DES, Figure 4C), consistent with prior studies.^{17,18}

Quantitative assessment of near-infrared fluorescence-fibrin and optical coherence tomography coverage relationships in bare metal stent and drug-eluting stent healing

Near-infrared fluorescence-fibrin and OCT-coverage stent strut data of Days 7 and 28 BMS and DES at edges were analysed and further classified into one of four groups: NIRF-fibrin negative and OCT-covered, identifying healed stent struts; or NIRF-fibrin positive, OCT-uncovered; NIRF-fibrin positive, OCT-covered; or NIRF-fibrin negative, OCT-uncovered; these latter three groups identifying unhealed stent struts. The data presented in Figure 5 demonstrates that in subacute and late timepoints after stent implantation, a significant percentage of OCT-covered stent struts is NIRF fibrin positive and thus can be considered to be unhealed (Figure 5, yellow groups). In addition, the proportion

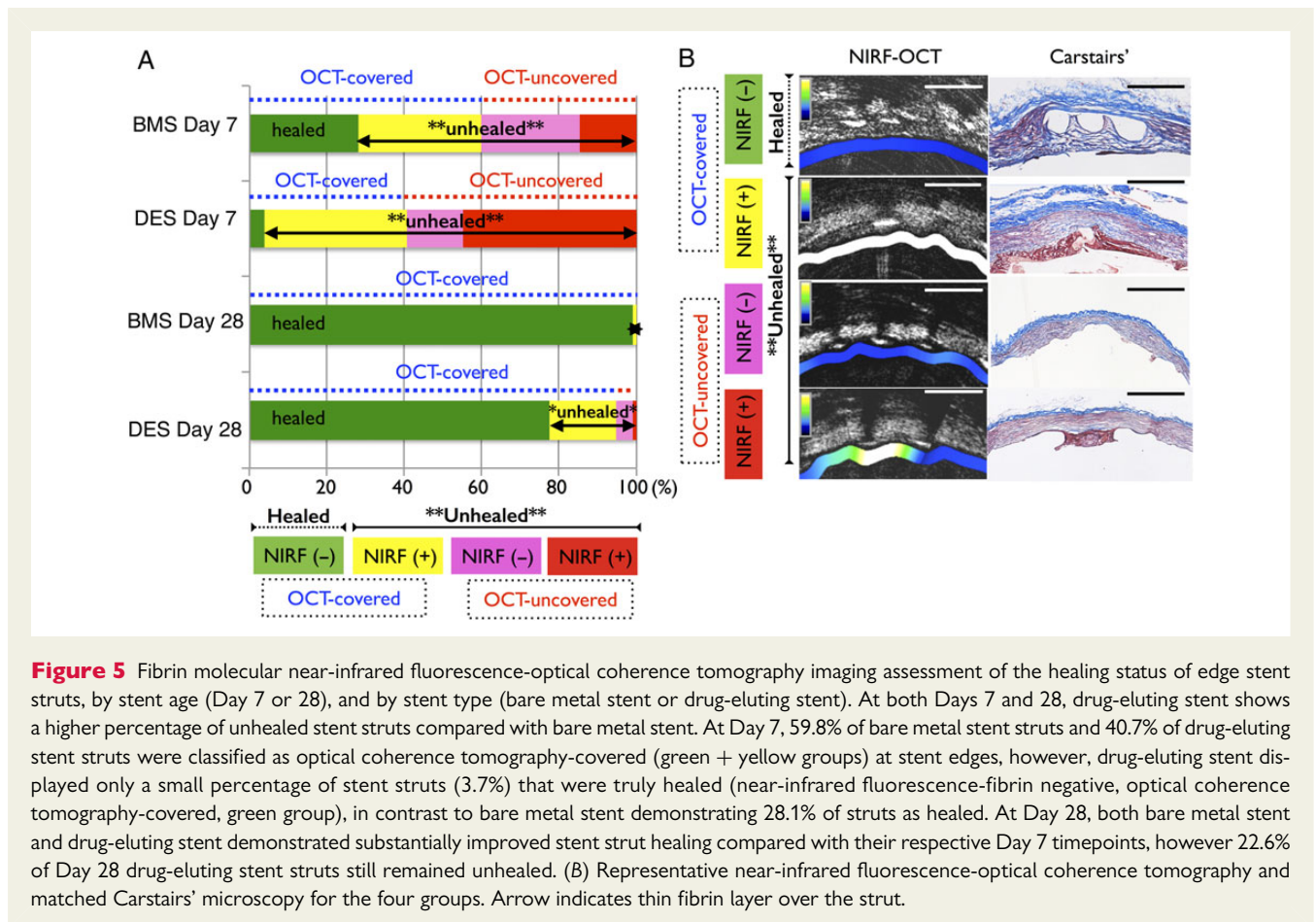


Figure 5 Fibrin molecular near-infrared fluorescence-optical coherence tomography imaging assessment of the healing status of edge stent struts, by stent age (Day 7 or 28), and by stent type (bare metal stent or drug-eluting stent). At both Days 7 and 28, drug-eluting stent shows a higher percentage of unhealed stent struts compared with bare metal stent. At Day 7, 59.8% of bare metal stent struts and 40.7% of drug-eluting stent struts were classified as optical coherence tomography-covered (green + yellow groups) at stent edges, however, drug-eluting stent displayed only a small percentage of stent struts (3.7%) that were truly healed (near-infrared fluorescence-fibrin negative, optical coherence tomography-covered, green group), in contrast to bare metal stent demonstrating 28.1% of struts as healed. At Day 28, both bare metal stent and drug-eluting stent demonstrated substantially improved stent strut healing compared with their respective Day 7 timepoints, however 22.6% of Day 28 drug-eluting stent struts still remained unhealed. (B) Representative near-infrared fluorescence-optical coherence tomography and matched Carstairs' microscopy for the four groups. Arrow indicates thin fibrin layer over the strut.

of unhealed stent struts remained significantly higher in DES compared with BMS at both Day 7 ($P < 0.001$) and Day 28 ($P < 0.05$).

Discussion

A key finding of this study is that a significant portion of OCT-covered stent struts may be actually covered by fibrin and are therefore unhealed, particularly earlier on after stenting. Specifically, over 90% of OCT-covered edge DES struts at Day 7, corresponding to the 1 month timepoint in humans, were positive for fibrin, a pro-thrombotic interface that mediates stent thrombosis.¹⁻³ At Day 28, corresponding to the 6–12 months timepoint in humans, combined NIRF-OCT determined that 23% of DES edge stents struts were unhealed—four times the percentage identified by standalone OCT (Figure 5A). The overall results demonstrate that intravascular NIRF fibrin molecular imaging can improve the identification of unhealed clinical coronary stents by clarifying whether OCT tissue coverage represents fibrin *in vivo*.

Optical coherence tomography is a promising approach to identify unhealed stents lacking tissue coverage, however, standalone OCT does not accurately distinguish between stent coverage by endothelium/smooth muscle cells (physiological stent healing) from coverage by prothrombotic fibrin, which indicates an unhealed stent.⁶ We observed a substantial proportion of OCT-covered stent struts are actually covered by fibrin (Figure 5). Therefore, a

subset of OCT-covered stent struts is actually *unhealed*, rather than healed. These *in vivo* findings extend the *ex vivo* study by Nakano *et al.* that demonstrated standalone OCT misclassification of healed stents occurs due to coverage by fibrin and inflammatory cells.⁶ Moreover, the observed mismatches between OCT and NIRF fibrin imaging fundamentally changes the perspective on whether such an OCT-covered stent could be prone to stent thrombosis. This finding is of substantial importance for ongoing clinical standalone OCT-based trials—which are predicated on the concept that tissue coverage of a stent means that a stent is healed and carries a low risk of stent thrombosis. The NIRF findings herein demonstrate that caution may be needed in interpreting the healing state of stents by standalone OCT, particularly in the subacute post-implantation period where unhealed stents are more prevalent.

While OCT grayscale intensity differences might identify fibrin,¹⁸ grayscale intensity was similar between DES and BMS in our study, despite DES having significantly higher fibrin content than BMS, further strengthening the value of NIRF molecular imaging to identify fibrin-rich unhealed stent struts. In addition, OCT stent strut coverage analysis is highly time-consuming (hours per individual stent), limiting its application in point-of-care analysis.¹⁹ In contrast, 2D NIRF fibrin maps (e.g. Figure 1A) readily display fibrin-rich areas on stents *in vivo*, NIRF molecular imaging powerfully complements standalone OCT structural imaging.

Pathophysiologically, NIRF-OCT fibrin-structural imaging provided new insights into differences in DES and BMS healing. Serial NIRF-OCT at subacute timepoints demonstrated that DES exhibited higher fibrin persistence than BMS out to Day 28 in rabbits, consistent with prior histopathological data.¹⁵ These findings need to be taken into context with studies of acute thrombus formation. We and others have shown, using these very same stents, that the coatings associated with DES are not inherently thrombogenic when evaluated in the acute setting associated with implantation and before drug release.¹³ This still remains the case. What we now show is that as DES elute their drug, there is a signal of increased subacute fibrin deposition that diminishes over time. Collectively, these data reinforce three timeperiods where implanted stents may be susceptible to thrombosis: an acute period related to surface effects and strut dimensions; a subacute period related to concentration of drug in local vicinities; and a third period related to a stunted or incomplete vascular healing response.

Although extrapolating healing rates from rabbits to humans is approximate, prior reports demonstrate that vascular healing in rabbits occurs 5–6 times faster than humans, and propose that Days 7 and 28 in rabbits correspond to 1 month and 6–12 months in humans, respectively.¹⁶ While current clinical guidelines indicate that 6–12 months of DAPT may be sufficient for prevention of DES thrombosis,²⁰ the recent DAPT study suggests that extended anti-platelet therapy of 30 months is beneficial.⁴ Therefore, the optimal duration of DAPT for coronary stents still remains unknown. Accordingly, the accurate identification of unhealed coronary stents could offer substantial value in guiding the duration of DAPT.

Clinical translation

The current study significantly advances the potential for intracoronary molecular imaging of fibrin deposition on stents. While an earlier study described the feasibility of imaging fluorescently coated clots placed on stents *ex vivo*,⁷ the present study provides the first demonstration that stent fibrin deposition can be imaged *in vivo* using an injectable NIRF molecular imaging agent, FTP11-CyAm7. As an MRI version of FTP11-CyAm7 has already been tested in Phase II trials,¹¹ and NIR fluorophores such as indocyanine green are clinically approved, the fibrin NIRF molecular imaging agent has substantial translational potential. From a catheter standpoint, clinical intracoronary testing of an NIRF-OCT catheter has already been initiated.²¹ These encouraging developments suggest that clinical NIRF molecular imaging of fibrin deposition on stents may be feasible in the near future.

Stent thrombosis remains a highly morbid, persistent complication of BMS and DES, and while despite long-term DAPT reduces stent thrombosis, thrombosis risk remains, and moreover appears to increase quickly after cessation of DAPT.^{1,4} The ability to image fibrin deposition on stents could therefore have several important applications. First, identifying fibrin-bearing stents might better predict the risk of stent thrombosis, motivating a re-review of optimal DAPT choices and duration, and selection for novel stent healing approaches. Second, fibrin imaging might prove to be a valuable surrogate endpoint for clinical trials evaluating new pro-healing stents and pharmacotherapies designed to reduce stent thrombosis.

Study limitations

As with other studies of rabbit stent healing,¹⁵ coronary stents were implanted into the normal aorta in rabbits without atherosclerotic plaque or curvature, as opposed to human coronary arteries. Iliac arteries, generally used in preclinical stent healing studies,¹⁵ were not stented due to limited repeated vascular access from femoral arteries, and to allow direct comparison between two stents within one pullback. While determining the precise mechanisms underlying enhanced fibrin deposition at the stent edges is beyond the scope of this manuscript, future studies will utilize computational fluid dynamic models²² to explore this issue. As light cannot penetrate through metallic stent struts, NIR fluorophores beneath metallic stent struts will not be detected by intravascular fluorescence reflectance imaging. Finally, delayed healing is only one feature underlying stent thrombosis, and other factors such as blood thrombogenicity and neoatherosclerosis will need to be integrated with NIRF-OCT fibrin imaging.

Conclusions

Intravascular NIRF fibrin molecular imaging improves the detection of unhealed stents by specifically determining whether OCT tissue coverage reflects fibrin deposition. Compared with NIRF-OCT, standalone OCT over-classifies stents as healed, even at subacute timepoints after stent implantation. Intravascular fibrin NIRF-OCT may ultimately help better identify stents at risk for stent thrombosis.

Supplementary material

Supplementary Material is available at *European Heart Journal* online.

Authors' contributions

T.H. performed statistical analysis; F.A.J., G.J.T., J.M. handled funding and supervision; T.H., G.U. acquired the data; F.A.J., G.J.T. conceived and designed the research; T.H., G.U., F.J. drafted the manuscript; E.R.E., G.J.T., F.A.J. made critical revision of the manuscript for key intellectual content.

Acknowledgements

We acknowledge Hongki Yoo, PhD for assistance with NIRF-OCT imaging, and Ashok Khatri, PhD and the MGH Peptide Core for the support of synthesis of imaging agent.

Funding

NIH R01HL108229 and R01HL122388 (F.A.J.), American Heart Association (#13POST14640021 to T.H.; #13GRNT17060040 to F.A.J.), MGH ECOR Support Fund (F.A.J.), and the Kanae Foundation for Research Abroad (T.H.). E.R.E. was supported in part by NIH R01GM49039. NIH R01HL093717 (G.J.T., for development of the imaging devices); CIMIT (F.A.J. and G.J.T., for development of the imaging devices).

Conflict of interest: F.A.J. receives sponsored research from Merck, Kowa, and Siemens, and nonfinancial research support from Boston Scientific. Massachusetts General Hospital has a patent licensing

arrangement with Terumo and Canon Corporations. G.J.T. (Terumo, Canon) and F.A.J. (Canon) have the right to receive licensing royalties through this licensing arrangement. G.J.T. receives consulting income from Samsung. G.J.T.'s lab receives sponsored research from Canon and InfraRedx and catheter components from Terumo.

References

- Claessen BE, Henriques JP, Jaffer FA, Mehran R, Piek JJ, Dangas GD. Stent Thrombosis: a clinical perspective. *JACC Cardiovasc Interv* 2014;**7**:1081–1092.
- Joner M, Finn AV, Farb A, Mont EK, Kolodgie FD, Ladich E, Kutys R, Skorija K, Gold HK, Virmani R. Pathology of drug-eluting stents in humans: delayed healing and late thrombotic risk. *J Am Coll Cardiol* 2006;**48**:193–202.
- Finn AV, Joner M, Nakazawa G, Kolodgie F, Newell J, John MC, Gold HK, Virmani R. Pathological correlates of late drug-eluting stent thrombosis: strut coverage as a marker of endothelialization. *Circulation* 2007;**115**:2435–2441.
- Mauri L, Kereiakes DJ, Yeh RW, Driscoll-Shempp P, Cutlip DE, Steg PG, Normand SL, Braunwald E, Wiviott SD, Cohen DJ, Holmes DR Jr, Krucoff MW, Hermiller J, Dauerman HL, Simon DI, Kandzari DE, Garratt KN, Lee DP, Pow TK, Ver Lee P, Rinaldi MJ, Massaro JM, Investigators DS. Twelve or 30 months of dual antiplatelet therapy after drug-eluting stents. *N Engl J Med* 2014;**371**: 2155–2166.
- Murata A, Wallace-Bradley D, Tellez A, Alviar C, Aboodi M, Sheehy A, Coleman L, Perkins L, Nakazawa G, Mintz G, Kaluza GL, Virmani R, Granada JF. Accuracy of optical coherence tomography in the evaluation of neointimal coverage after stent implantation. *JACC Cardiovasc Imaging* 2010;**3**:76–84.
- Nakano M, Vorpahl M, Otsuka F, Taniwaki M, Yazdani SK, Finn AV, Ladich ER, Kolodgie FD, Virmani R. Ex vivo assessment of vascular response to coronary stents by optical frequency domain imaging. *JACC Cardiovasc Imaging* 2012;**5**: 71–82.
- Yoo H, Kim JW, Shishkov M, Namati E, Morse T, Shubochkin R, McCarthy JR, Ntziachristos V, Bouma BE, Jaffer FA, Tearney GJ. Intra-arterial catheter for simultaneous microstructural and molecular imaging *in vivo*. *Nat Med* 2011;**17**: 1680–1684.
- McCarthy JR, Patel P, Botnaru I, Haghayeghi P, Weissleder R, Jaffer FA. Multimodal nanoagents for the detection of intravascular thrombi. *Bioconjugate Chemistry* 2009; **20**:1251–1255.
- Ughi GJ, Verjans J, Fard AM, Wang H, Osborn E, Hara T, Mauskopf A, Jaffer FA, Tearney GJ. Dual modality intravascular optical coherence tomography (OCT) and near-infrared fluorescence (NIRF) imaging: a fully automated algorithm for the distance-calibration of NIRF signal intensity for quantitative molecular imaging. *Int J Cardiovasc Imaging* 2015;**31**:259–268.
- Hara T, Bhayana B, Thompson B, Kessinger CW, Khatri A, McCarthy JR, Weissleder R, Lin CP, Tearney GJ, Jaffer FA. Molecular imaging of fibrin deposition in deep vein thrombosis using fibrin-targeted near-infrared fluorescence. *JACC Cardiovasc Imaging* 2012;**5**:607–615.
- Vymazal J, Spuentrup E, Cardenas-Molina G, Wiethoff AJ, Hartmann MG, Caravan P, Parsons EC Jr. Thrombus imaging with fibrin-specific gadolinium-based MR contrast agent EP-2104R: results of a phase II clinical study of feasibility. *Invest Radiol* 2009;**44**:697–704.
- Jaffer FA, Verjans JW. Molecular imaging of atherosclerosis: clinical state-of-the-art. *Heart* 2014;**100**:1469–1477.
- Kolandaivelu K, Swaminathan R, Gibson WJ, Kolachalama VB, Nguyen-Ehrenreich KL, Giddings VL, Coleman L, Wong GK, Edelman ER. Stent thrombogenicity early in high-risk interventional settings is driven by stent design and deployment and protected by polymer-drug coatings. *Circulation* 2011;**123**: 1400–1409.
- Joner M, Nakazawa G, Finn AV, Quee SC, Coleman L, Acampado E, Wilson PS, Skorija K, Cheng Q, Xu X, Gold HK, Kolodgie FD, Virmani R. Endothelial cell recovery between comparator polymer-based drug-eluting stents. *J Am Coll Cardiol* 2008;**52**:333–342.
- Nakazawa G, Nakano M, Otsuka F, Wilcox JN, Melder R, Pruitt S, Kolodgie FD, Virmani R. Evaluation of polymer-based comparator drug-eluting stents using a rabbit model of iliac artery atherosclerosis. *Circ Cardiovasc Interv* 2011;**4**:38–46.
- Virmani R, Kolodgie FD, Farb A, Lafont A. Drug eluting stents: are human and animal studies comparable? *Heart* 2003;**89**:133–138.
- Malle C, Tada T, Steigerwald K, Ughi GJ, Schuster T, Nakano M, Massberg S, Jehle J, Guagliumi G, Kastrati A, Virmani R, Byrne RA, Joner M. Tissue characterization after drug-eluting stent implantation using optical coherence tomography. *Arterioscler Thromb Vasc Biol* 2013;**33**:1376–1383.
- Templin C, Meyer M, Muller MF, Djonov V, Hlushchuk R, Dimova I, Flueckiger S, Kronen P, Sidler M, Klein K, Nicholls F, Ghadri JR, Weber K, Paunovic D, Corti R, Hoerstrup SP, Luscher TF, Landmesser U. Coronary optical frequency domain imaging (OFDI) for *in vivo* evaluation of stent healing: comparison with light and electron microscopy. *Eur Heart J* 2010;**31**:1792–1801.
- Adriaenssens T, Ughi GJ, Dubois C, Onsea K, De Cock D, Bennett J, Wiyono S, Vanhaverbeke M, Sinnaeve P, Belmans A, D'Hooge J, Desmet W. Automated detection and quantification of clusters of malapposed and uncovered intracoronary stent struts assessed with optical coherence tomography. *Int J Cardiovasc Imaging* 2014;**30**:839–848.
- Authors/Task Force Members, Windecker S, Kolh P, Alfonso F, Collet JP, Cremer J, Falk V, Filippatos G, Hamm C, Head SJ, Juni P, Kappetein AP, Kastrati A, Knuuti J, Landmesser U, Laufer G, Neumann FJ, Richter DJ, Schauerte P, Sousa Uva M, Stefanini GG, Taggart DP, Torracca L, Valgimigli M, Wijns W, Witkowski A. 2014 ESC/EACTS Guidelines on myocardial revascularization: The Task Force on Myocardial Revascularization of the European Society of Cardiology (ESC) and the European Association for Cardio-Thoracic Surgery (EACTS) Developed with the special contribution of the European Association of Percutaneous Cardiovascular Interventions (EAPCI). *Eur Heart J* 2014;**35**:2541–2619.
- Ughi G, Wang H, Gardecki JA, Gerbaud E, Fard AM, Hamidi E, Jacques-Vacas P, Rosenberg M, Jaffer FA, Tearney GJ. First-In-Human Dual-Modality OCT and Near-Infrared Autofluorescence Imaging of Coronary Artery Disease. *JACC Cardiovascular Imaging* (in press).
- Balakrishnan B, Tzafiriri AR, Seifert P, Groothuis A, Rogers C, Edelman ER. Strut position, blood flow, and drug deposition: implications for single and overlapping drug-eluting stents. *Circulation* 2005;**111**:2958–2965.